Journal of Alloys and Compounds 681 (2016) 307–315

Contents lists available at ScienceDirect

Journal of Alloys and Compounds

journal homepage: http://www.elsevier.com/locate/jalcom

Formation of silver nanoparticles in silicate glass using excimer laser radiation: Structural characterization by HRTEM, XRD, EXAFS and optical absorption spectra

Maximilian Heinz [a], Vasiliy V. Srabionyan [b], Aram L. Bugaev [b], Vasiliy V. Pryadchenko [b], Egor V. Ishenko [b], Leon A. Avakyan [b], Yan V. Zubavichus [c], Jürgen Ihlemann [d], Jörg Meinertz [d], Eckhard Pippel [e], Manfred Dubiel [a], Lusegen A. Bugaev [b, *]

[a] Department of Physics, University of Halle-Wittenberg, Von-Danckelmann-Platz 3, D-06120 Halle, Germany
[b] Department of Physics, Southern Federal University, Zorge Str., 5, 344090 Rostov-on-Don, Russia
[c] Kurchatov Center for Synchrotron Radiation and Nanotechnology, National Research Centre "Kurchatov Institute", Academic Kurchatov Sq. 1, 123182 Moscow, Russia
[d] Laser-Laboratorium Göttingen, Hans-Adolf-Krebs-Weg 1, D-37077 Göttingen, Germany
[e] Max-Planck-Institute of Microstructure Physics, Weinberg 2, D-06120 Halle, Germany

ARTICLE INFO

Article history:
Received 23 December 2015
Received in revised form
19 April 2016
Accepted 20 April 2016
Available online 23 April 2016

Keywords:
Nanostructured materials
Laser processing
Optical materials
Surface plasmon resonance
Optical spectroscopy
EXAFS

ABSTRACT

Plasmonic silver nanostructures in surfaces of soda-lime silicate glasses were generated using $Ag^+ \leftrightarrow Na^+$ ion exchange and UV laser irradiation (ArF laser, 193 nm) with different number of *ns* laser pulses (from 2 to 5000). To identify the correlations between the optical properties (surface plasmon resonance (SPR) parameters) and atomic structure of silver nanoparticles and their agglomerations, characterization of the samples was performed by HRTEM, XRD, optical absorption in visible range and Ag *K*-edge EXAFS spectra. Analysis of the optical spectra was performed using a Mie theory approach, accounting for the most plausible defect centers in silicate glass like hole trap centers and non-bridging oxygen hole centers. Processing of Ag *K*-edge EXAFS yielded values of Ag-Ag and Ag-O interactions averaged over ionic and neutral states of silver. The consistent treatment of HRTEM and XRD data, the behavior of features in optical spectra and the obtained dependence of Ag-Ag and Ag-O structural parameters upon the number of laser pulses enabled to suggest a mechanism of plasmonic Ag nanoparticles formation in silicate glass under UV laser irradiation.

1. Introduction

Formation of metal nanoparticles in dielectric matrices has been extensively studied because these nanocomposite materials exhibit linear and non-linear optical properties, which are determined by the surface plasmon resonance (SPR) of nanoparticles [1–5]. Silver nanoparticles in glasses are attracting particular attention since the wavelength of their SPR (λ_{pl}) is distinctively separated from the wavelengths of interband absorption [5], making such materials promising candidates for applications in optoelectronics and nanoplasmonics. Typically, silver nanoparticles in sodium silicate glasses are prepared by $Ag^+ \leftrightarrow Na^+$ ion exchange process and subsequent thermal treatment [6–9]. However, this method does not allow creating nanoscaled arrays of particles localized in a certain way.

In our previous work [10] to obtain spatially specific precipitation of nanoparticles (e. g. line structures) in glass surfaces laser irradiation by means of ultraviolet laser irradiation (193 nm and 405 nm) below the ablation threshold was implemented. Usually, an IR laser was used for particles formation providing the diffusion and reaction processes on the basis of heating of the glass. Besides, silver nanoparticles in soda-lime glass were formed by visible and UV laser radiation [4,11–13] between 244 and 1064 nm. Here, a UV laser of 193 nm was used to produce high-resolution patterning with the minimum of damage to the glass surface. However, UV radiation, depending on the laser parameters, can lead to the reduction of size or dissolution of nanoparticles [14] and to their instability even at room temperature. These processes can occur

* Corresponding author.
E-mail address: bugaev@sfedu.ru (L.A. Bugaev).

http://dx.doi.org/10.1016/j.jallcom.2016.04.214
0925-8388/

since UV irradiation of glass induces the creation of various defect centers [15,16], which results both in the enhancement of particles formation and in the recombination processes giving a decrease in particles concentration. It was also shown that using pulsed UV laser the formation of stable nanoparticles can be obtained in some cases without additional thermal treatment [17]. Therefore, to obtain stable nanoparticles with specific characteristics of the SPR such as λ_{pl}, full width at half maximum (FWHM), dephasing time, it is necessary, to examine the dependences of these characteristics upon the parameters of the laser irradiation and to obtain values of these parameters that provide stability of the forming nanoparticles in glasses. These characteristics of the SPR depend in turn on the size, form, atomic structure of nanoparticles and dielectric properties of the surrounding matrix [18,19].

In this work, the formation of silver nanoparticles near the surface of sodium silicate glasses is performed by excimer laser beam irradiation (ArF, 193 nm) with different numbers of nanosecond pulses (from 2 to 5000) and is studied using X-ray diffraction (XRD), optical absorption spectroscopy, high-resolution transmission electron microscopy (HRTEM) and Ag *K*-edge extended X-ray absorption fine structure (EXAFS). In Sec. 2 the procedure for silver particles preparation by excimer laser radiation is presented together with description of optical, HRTEM, XRD and EXAFS measurements. Analysis of HRTEM micrographs and XRD profiles, interpretation of optical absorption spectra, which was performed taking into account the properties of color centers in silicate glasses and the results of application of Mie theory [20], are presented in Sec. 3 together with the structural parameters of Ag-Ag and Ag-O interactions obtained from EXAFS. The consistent analysis of XRD data, changes in optical absorption spectra and corresponding dependencies of Ag-Ag and Ag-O bonds parameters, derived from EXAFS of samples treated with different number of laser pulses, enabled us to propose a mechanism of silver nanoparticles formation in sodium silicate glass under UV laser irradiation.

2. Experimental

2.1. Synthesis of samples

For this work, soda-lime silicate float glass of the following composition (main components in weight-%): 72.3% SiO_2, 13.3% Na_2O, 4.3% MgO, 8.8% CaO, 0.5% Al_2O_3, 0.4% K_2O was used. At first the glass slides (thickness 1 mm) were doped with silver ions by means of a silver/sodium ion exchange ($Ag^+ \leftrightarrow Na^+$). To this end, the glass slides were immersed into a molten 95 wt.-% $NaNO_3$/5 wt.-% $AgNO_3$ salt bath at a temperature of 330 °C for 20 min. Then, ion exchanged glass slides were irradiated by an ArF-excimer laser (Lambda Physik LPX 315; wavelength 193 nm, 20 ns pulse duration) on the tin bath side to form silver nanoparticles. The tin side of the float glass was used for particle formation because of the amount of Sn^{+2} ions in addition to Fe^{2+} ions [21,22]. The iron concentration is constant inside the whole glass matrix. These Sn and Fe ions are able to act as reducing agents in order to create neutral Ag atoms that is a precondition for the formation of Ag nanoparticles [10]:

$$Fe^{2+} + Ag^{+} \rightarrow Fe^{3+} + Ag^{0} \quad (1)$$

$$Sn^{2+} + 2\,Ag^{+} \rightarrow Sn^{4+} + 2\,Ag^{0} \quad (2)$$

Furthermore, there is an increased absorption of the UV laser light due to tin ions. That's why the irradiation of the tin bath side yields more significant laser marks and an increased absorption band in comparison to the same experiments at the air side (Fig. 1). This effect is similar for all other pulse numbers. The laser

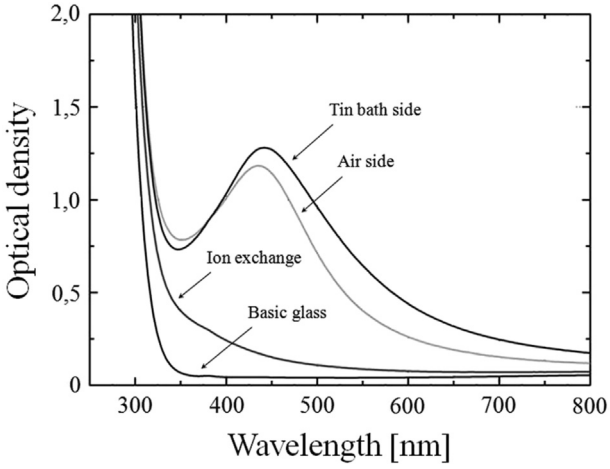

Fig. 1. Optical absorption spectra of the base glass, the ion-exchanged glass and as a result of the laser irradiation of the air side and the tin bath side of Sample 5000.

irradiation was performed at a fluence of approximately 100 mJ/cm^2 and a pulse repetition frequency of 10 Hz. The number of laser pulses was varied from 2 to 5000. The size of the laser spots was approximately 5 × 5 mm^2 to 10 × 10 mm^2. For clarity and simplicity of notations, the samples prepared by means of 2, 5, 10, 20, 100, 500, 1000 and 5000 laser pulses will be referred to as Sample 2, Sample 5, Sample 10, Sample 20, Sample 100, Sample 500, Sample 1000 and Sample 5000 respectively.

Fig. 2a shows a microscope image of a cross-sectional preparation to demonstrate the penetration depth of the silver ions after the ion exchange (pale yellow area) as well as the zone of formation of silver nanoparticles (dark yellow and brown area). It's apparent that the penetration depth of the silver ions due to the ion exchange is approximately 5 μm and the silver nanoparticles are formed in a very thin surface layer of approximately 2 μm only.

2.2. Characterization of nanoparticles by optical spectroscopy and HRTEM

Absorption spectra were measured with a UV/Vis/NIR spectrometer (Perkin Elmer, Lambda 900) in the range from 250 nm to 800 nm. To compare the experimental absorption spectra with simulations according to Mie theory, the extinction coefficient $k(\lambda)$ as a function of wavelength λ was calculated according to eq. (3):

$$k(\lambda) = (\ln 10)\cdot\frac{OD(\lambda) - OD_{basic\ glass}(\lambda)}{d} \quad (3)$$

where $OD(\lambda)$ denotes the measured optical density and $OD(\lambda)_{basic\ glass}$ represents the optical density of the untreated float glass. By assuming a thickness d of 2 μm the extinction coefficient of the particle layer can be calculated.

HRTEM examination to evaluate size, size distribution and penetration depth of silver particles was done for two selected samples (Sample 10 and 5000) by means of a FEI Titan 80–300 operating at 300 kV. To this end, cross-section preparation was applied including mechanical grinding, polishing and ion beam etching.

2.3. XRD and EXAFS measurements

X-ray powder diffraction data were collected at the Swiss-Norwegian Beamline (BM01B) of the European Synchrotron Radiation Facility (ESRF) using 0.50523 Å radiation. The samples, having

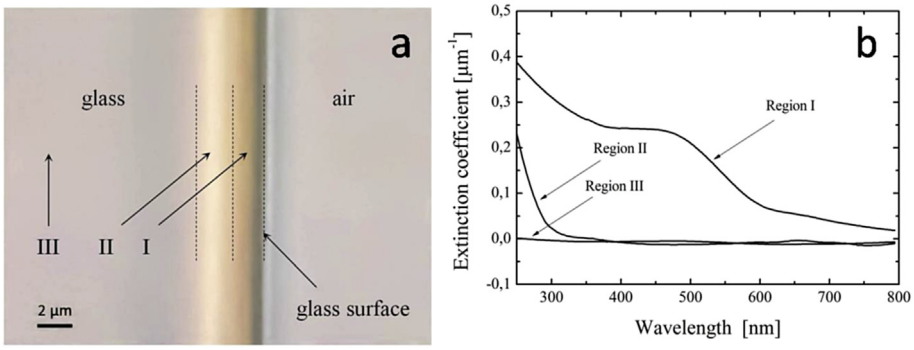

Fig. 2. (a) – Microscope image of the cross-sectional glass sample (thickness of 9 µm) as result of silver/sodium ion exchange (330 °C, 20 min) and subsequent ArF laser irradiation; (b) – optical spectra measured by a microscope spectral photometer (size of the measured area: 0.5 × 40 µm^2) of region of particle formation (I), of penetration depth of Ag ions (II) and unmodified base glass (III).

a rectangular shape, were oriented perpendicular to the 1 × 1 mm^2 X-ray beam. A CMOS-Dexela 2D detector was placed at 244.4 mm distance from the sample. The setup allowed to collect scattered photons in the 2θ range up to 50°. For each sample, 20 images with 5 s acquisition time were collected alternating with 20 dark images. Subsequent averaging, dark current subtraction and integration was performed in PyFAI software in order to obtain $I(2\theta)$ profiles. Jana2006 code was used for simulation of theoretical XRD profiles and comparison with experimental data.

Ag *K*-edge EXAFS spectra were acquired at the Structural Materials Science beamline of the Kurchatov Synchrotron Radiation Source (NRC "Kurchatov Institute", Moscow, Russia) in fluorescence yield mode using a Si avalanche photodiode as a detector at room temperature. The incident intensity was monitored with an Ar-filled ion chamber. In order to improve the signal-to-noise statistics several scans for each sample were measured and averaged. The total data collection time was 3–4 h per sample.

For some samples Ag *K*-edge EXAFS were re-measured at BM01B beamline of ESRF in transmission mode using ionization chambers from 25.4 to 26.1 keV. The samples were positioned in the same geometry as described for the XRD experiments. Energy scanning was performed in continuous scanning mode. A silver foil was used as reference sample and was measured simultaneously with every sample for energy calibration.

3. Results and discussion

3.1. TEM and optical spectroscopy

Fig. 3a shows a TEM image of Sample 5000. It is obvious that the sample contains two different types of Ag precipitations. There are separated small Ag nanoparticles of sizes between 1 and 3 nm and larger species of sizes ≥5 nm, which consist of agglomerations of smaller Ag nanoparticles (see Fig. 3b and 3c). All small silver nanoparticles must have a crystalline structure [23]. Fig. 3b and 3c demonstrate varied distances between small single Ag particles inside the agglomerations. In either case, one can expect interactions among these nanoparticles. The particle density $N(R)$ of single Ag particles (1–3 nm sizes) surrounded by the glass matrix and of the larger agglomerations (5–16 nm) is shown in Fig. 4a. It is quite obvious that the total particle density N_0 of separated nanoparticles (that is the total number of particles per volume) is much higher than that of the larger agglomerations. It has to be also noted that some increase in the density of the small particles has been observed during TEM investigations due to the electron beam irradiation. The final particle density of smaller particles was of the order of 10^{18} cm^{-3}, so that the real concentration as generated by laser irradiation should be less. HRTEM investigations of Sample 10 showed similar results with respect to both the size and volume concentration C_V of separated Ag nanoparticles (approximately $0.3\cdot10^{-2} - 0.5\cdot10^{-2}$) that is the volume of nanoparticles in comparison to the total volume.

Fig. 4b represents a fit of the size distribution of agglomerations assuming a log-normal distribution with size parameter R_0 (mean

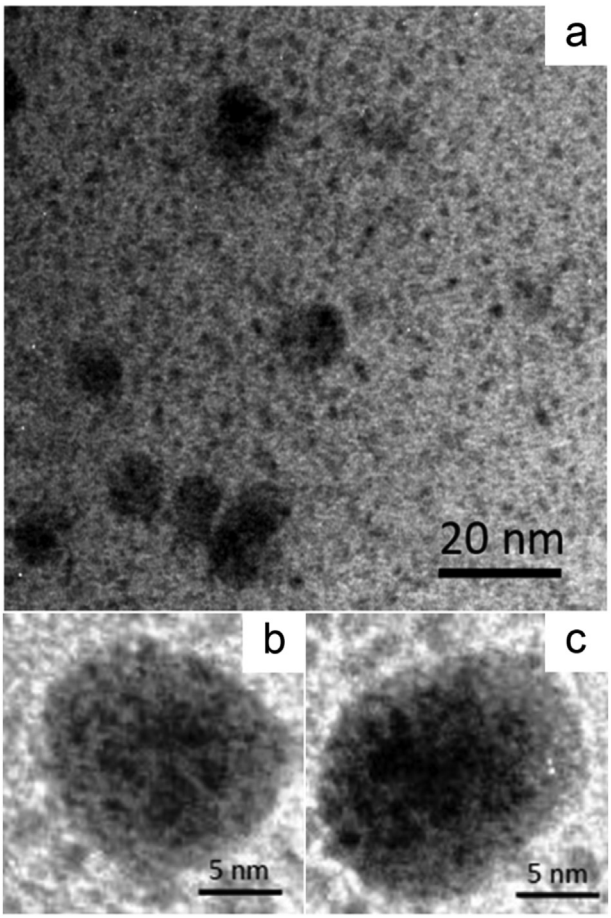

Fig. 3. TEM images for Sample 5000. (a) – Micrograph showing two types of crystalline Ag species: separated small nanoparticles (1–3 nm) and larger agglomerations; (b) and (c) – images of larger precipitations containing Ag demonstrate an inhomogeneous structure that can be interpreted as agglomerations of smaller Ag nanoparticles.

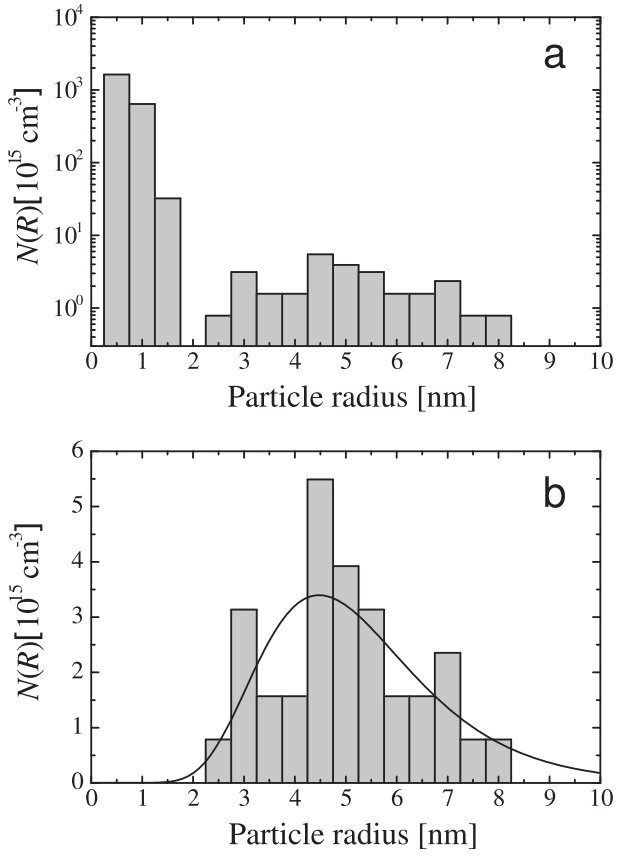

Fig. 4. (a): Particle size distributions obtained by TEM investigations of Sample 5000; (b): fit of the size distribution of the agglomerations (radius > 2.5 nm) in Sample 5000 according to a log-normal function. In (a) and (b) the step function as a result of counting the nanoparticles has been normalized.

size), width parameter σ and particle density N_0:

$$N(R) = \frac{N_0}{\sqrt{2\pi}\cdot\sigma}\cdot\frac{1}{R}\cdot e^{-\frac{\ln\left(\frac{R}{R_0}\right)^2}{2\sigma^2}} \quad (4)$$

where the values of R and R_0 are multiples of 1 nm. Concerning Sample 5000, the fit yields a size parameter of $R_0 = 5$ nm, a width parameter of $\sigma = 0.33$ nm, a particle density of $N_0 = 1.33\cdot10^{16}$ cm^{-3} and a volume concentration of $C_V \approx 1.1\cdot10^{-2}$ of agglomerations. It should be noted that the values for N_0 and C_V refer to the particle layer in the glass surface. The thickness of this layer is approximately 2 μm. Compared to Sample 5000, investigations of Sample 10 showed a diminished mean radius ($R_0 = 4.1$ nm) as well as a reduced volume concentration ($C_V \approx 0.6 \times 10^{-2}$) of agglomerations as calculated by a log-normal distribution according to Eq. (4). These results suggest that the size of agglomerations and their volume concentration increases with increasing number of applied UV laser pulses.

The extinction spectrum of Ag/Na ion-exchanged glasses (at the float side) is displayed in Fig. 5a and the spectra of Samples 10, 100, 500, 1000 and 5000 are presented in Fig. 5b. It should be noted that the extinction due to the base glass has been subtracted for all samples. The extinction spectra of ion-exchanged glasses should contain silver ions and neutral atoms, but Fig. 5a reveals that some defects are created in addition to these Ag species. Furthermore, it is obvious that up to 100 pulses (Samples 10 and 100) the spectra are characterized by a broadened absorption band with a maximum at ~450 nm, which should be attributed to various defect

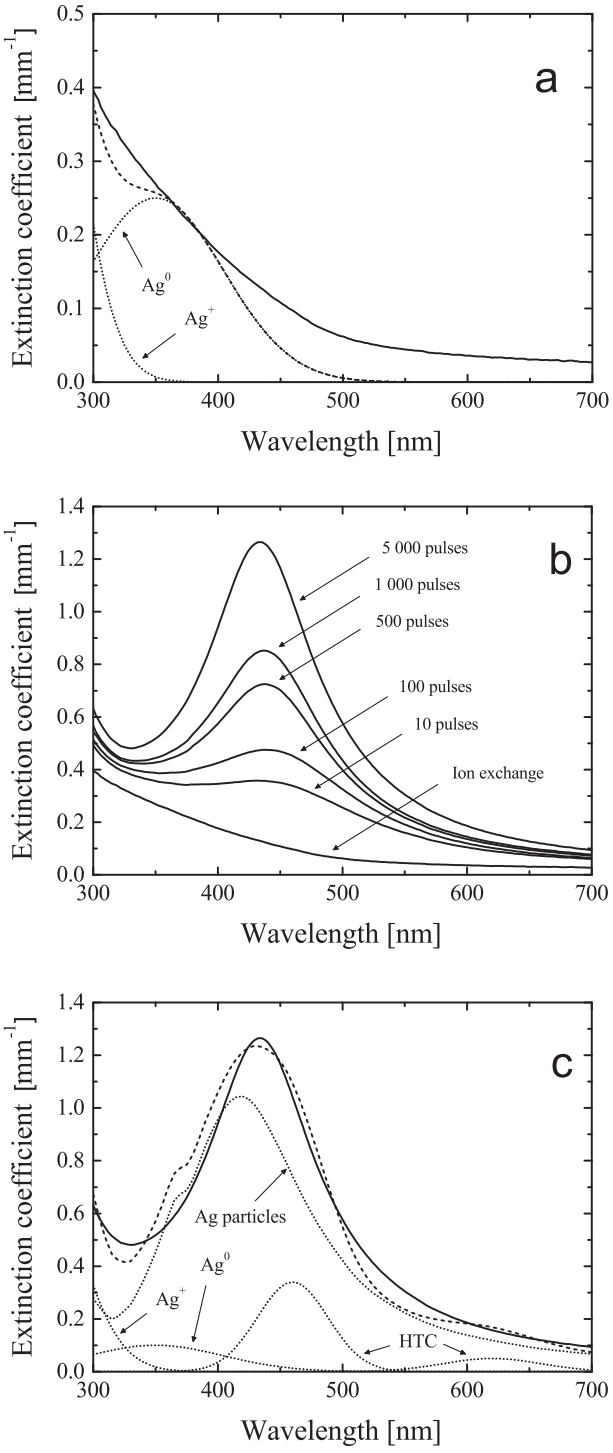

Fig. 5. Optical absorption spectra of the Ag/Na ion-exchanged glass samples (measured data – solid lines) together with theoretical calculations (dotted lines) assuming the simultaneous existence of silver ions, atoms, nanoparticles and hole trap centers. (a) – Spectrum of ion exchanged sample without laser irradiation; (b) – spectra of ion exchanged glass and Samples 10, 100, 500, 1000 and 5000; (c) – optical spectrum of Sample 5000 together with simulated spectra of the considered Ag species (dashed line represents the summation of all contributions).

centers, Ag ions and atoms, clusters and only some nanoparticle species. That means, the UV irradiation creates manifold defects and given that, it is difficult to identify the corresponding absorption phenomena. On the other hand, the spectra of Samples 500, 1000 and 5000 show a well-defined absorption peak that should be

dominated by SPR of silver nanoparticles with a decreasing amount of defect centers. The maximum of this plasmon resonance is shifted from 450 nm (500 pulses) to 435 nm (5000 pulses) with increasing number of applied UV laser pulses.

In order to identify the mechanisms of formation of Ag nanoparticles and possible aggregates therefrom, the measured extinction spectra should be simulated by absorption processes of possible defects generated by UV irradiation as well as by different configurations of Ag species, formed as the result of incorporation of silver by the Ag/Na ion exchange process. Thus, the optical spectra were simulated assuming the existence of silver ions (maximum of absorption at $\lambda \leq 240$ nm [24,25]) and of silver atoms (absorption at $\lambda \leq 350$ nm [26]) as well as of silver nanoparticles. Such calculation based on Mie theory [20] allowed to describe the experimental data in the low-wavelength range between 300 and 400 nm by the Ag ions and atoms and for longer wavelengths by the SPR of Ag species. However, the corresponding mean sizes of Ag nanoparticles were calculated as 30 nm, 24 nm and 14 nm for Samples 500, 1000 and 5000, respectively. These sizes of particles were not confirmed by the TEM experiments.

These calculations indicate the existence of clusters of nanoparticles forming coagulation aggregates. Kreibig and Quinten [20,27] have proposed a quasi-static approximation for many-pairs samples of Ag spheres with statistically isotropic distribution of orientations of pairs. The resulting absorption spectra should be calculated for a well-defined ratio R/D of radii (R) of nanoparticles to the center to center distance (D) between neighboring clusters or particles. Based on the TEM results, we calculated a mean value over all Ag particles for Sample 5000 of approximately $R/D = 0.35$. In addition, we assumed the existence of hole trap centers (HTC) at the non-bridging oxygen atoms when a Si-O-Si bond breaks due to irradiation with UV light [15,28,29]. Such hole centers generate absorption peaks at 430–450 nm and 620 nm. The results of simulations are shown in Fig. 5c using a mean Ag particle size of 3 nm. The volume concentration of the silver aggregates increases from $C_V \approx 1.6 \cdot 10^{-3}$ (Sample 100) to $C_V \approx 5.8 \cdot 10^{-3}$ (Sample 5000). These values are much smaller than those obtained by the TEM images because of the increase of the density of the small particles due to the electron beam irradiation during the TEM investigations, as already mentioned. As a result of the simulations only the volume concentration of the silver aggregates increases with the number of laser pulses, while the particle radius R and the center to center distance D remain constant. The obtained agreement between the simulated and the measured data permits to conclude that these calculations allow to describe the essential processes of formation of Ag particles in float glass surface containing silver, by means of ArF laser irradiation.

3.2. XRD characterization of samples

XRD patterns of Samples 2, 5, 10, 5000 are presented in Fig. 6a. The dominant peak in all patterns at angle 2θ ~8° corresponds to the silicate glass matrix. The weak features at 14, 20 and 24° are indicative of *f.c.c.* silver. The last was confirmed by comparison of experimental data for Sample 5000 with simulated patterns of *f.c.c.* silver shown in Fig. 6b. The peak width in the theoretical patterns was chosen according to the Debye-Scherrer equation and corresponds to particle sizes of 1.5 nm (blue) and 3 nm (orange). Comparison of theoretical and simulated patterns indicates that the angle positions of the main features of experimental spectra are in agreement with the theoretical ones.

The low signal to background ratio of the observed patterns does not allow performing Rietveld analysis. However, qualitative comparison of the widths of the features in the experimental XRD profiles with those in the theoretical ones (Fig. 6b) indicates that the crystalline size (particle size) of the silver nanoparticles probed by XRD does not exceed ~ 1.5 nm, which corresponds to a particle size D ~ 2 nm according to [30]. The ability of XRD to distinguish metal nanoparticles of such a small size is confirmed by the results of [31] where clearly-defined XRD reflections of *f.c.c.* silver were observed in silver nanoparticles with an average size of 2–4 nm, while nanoparticles ranged in 1–1.5 nm in diameter were not reflected in diffraction.

3.3. Discussion of particle sizes and expected bond lengths

The simulation of optical spectra in silicate glasses after $Ag^+ \leftrightarrow Na^+$ ion exchange and subsequent UV laser irradiation demonstrated that it is necessary to account for different plausible constructions of the silver atoms (e. g. color centers), which can be formed and absorb in the visible range at λ ~420–460 nm. The most suitable constructions are the well-known hole-trap centers (HTC) [28,29,32], clusters of neutral silver atoms Ag^0_n ($n = 2$–15 atoms) [33] and small silver nanoparticles of sizes < 1.5 nm, which cannot be observed by XRD. Furthermore, NBOHC should be considered as a result of excimer laser irradiation. These defects show absorption processes at 420 nm and 627 nm [17].

HTC and NBOHC defect centers exist to a small amount in silicate glass, especially in the near-surface region, independent of any irradiation processes. However, the formation of the new centers can be strongly enhanced by irradiation with UV, light, X-rays or γ-rays, which break Si–O–Si bonds [28]. Assuming the generation of additional HTC and NBOHC centers by UV laser irradiation and taking into consideration their corresponding optical absorptions, the optical spectra can be explained.

To examine silver particles formation under laser irradiation of glass in the presence of other species of silver (in small clusters, HTC and NBOHC defect centers) it is necessary to have estimates of corresponding Ag-Ag nearest neighbors distances ($R_{Ag\text{-}Ag}$), which can help to reveal if nanoparticles contribution (with $R_{Ag\text{-}Ag}$ ~ 2.87 Å) [23] are distinguished or not from these species by EXAFS analysis. The calculated values of $R_{Ag\text{-}Ag}$ in small clusters of silver atoms are presented in Sec. 3.4. To estimate values of $R_{Ag\text{-}Ag}$ in HTC and to reveal the stability of such a center, modeling by density functional theory (DFT) was performed.

HTC centers in Ag^+ – doped silicate glasses are characterized by a wide absorption line peaking at ~430–450 nm and a weaker line at ~620–650 nm [29]. According to the results of [28], one can suggest that in silicate glass the HTC are located near the network tetrahedrons SiO_4 with two or three non-bridging oxygen atoms and Ag^+ ions in the immediate neighborhood. Such a tetrahedron captures a hole forming different HTC, which are schematically presented in parts (a) – (c) of Fig. 7. Among them, structures (b) and (c) contain Ag^+-Ag^+ bonds, the presence of which can be confirmed by EXAFS at least indirectly. To reveal the stability of HTC structure (b) with two silver ions and to estimate the corresponding values of Ag-Ag and Ag-O distances, DFT modeling was performed using PBE exchange correlation functional [34] and Pople basis set 6-31G. The applied finite cluster approach [35] is efficient for charged systems since there is no need to introduce energy corrections to compensate for the interaction of charged neighbor cells, as is required when periodic boundary conditions are implemented. The obtained HTC structure presented in Fig. 7d, corresponds to scheme (b), and is characterized by the values of $R_{Ag^+\text{–}Ag^+} = 3.2$ Å and $R_{Ag^+\text{–}O} = 2.05$ Å. In this structure the hole is localized on O1 and O2 atoms.

For NBOHC centers, it is not known if silver ions or atoms are involved in defect configurations formed in Ag+ – doped glasses. However, it has been found that a NBOHC can act as reducing agent for silver ions [36]. That yields an increased number of nuclei for

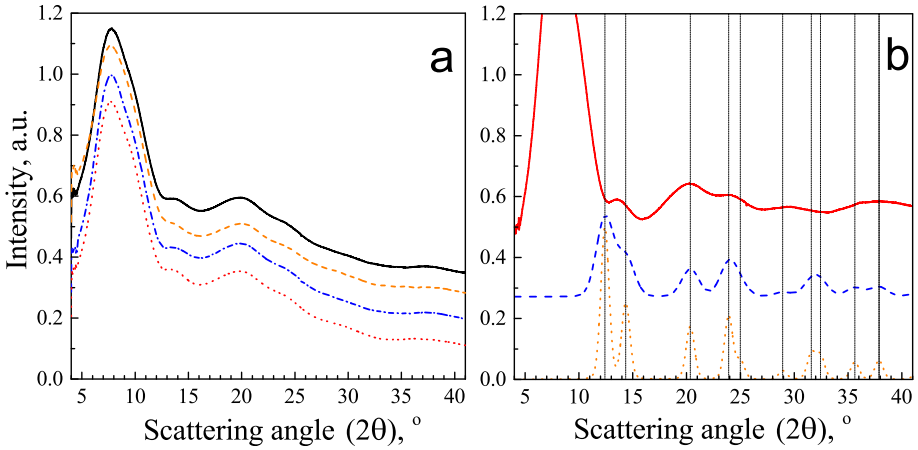

Fig. 6. (a): XRD patterns of samples after irradiation with 2 (black solid line), 5 (orange dashed line), 10 (blue dash-dotted line), and 5000 (red dotted line) UV laser pulses; (b): comparison of experimental pattern of Sample 5000 (red solid line) with theoretical patterns with peak widths corresponding to a grain size of 1.5 nm (blue dashed line) and 3 nm (light-brown dotted line). Dashed lines correspond to the positions of the silver *f.c.c.* reflections. Cell parameter for XRD simulations: $a = 4.045$ Å according to the results of EXAFS analysis (vide infra). For visualization purposes, a smooth background line was subtracted from the experimental curve in part b. (For interpretation of the references to colour in this figure legend, the reader is referred to the web version of this article.)

the precipitation of crystalline Ag nanoparticles similarly to the reaction with Fe and Sn ions. Therefore, these reactions cause a strongly enhanced concentration of Ag particles of small sizes and the formation of larger aggregates therefrom, these are the agglomerations as discussed above.

3.4. Structural parameters of Ag-Ag and Ag-O bonds obtained from EXAFS

In Fig. 8 the magnitudes of the Fourier-transforms (FT) $|F(R)|$ of experimental Ag *K*-edge EXAFS in Sample 20 (low number of pulses) and in Sample 5000 (largest number of pulses) are compared. As can be seen, the magnitude of the first peak, which corresponds to the contribution of Ag-O interactions, decreases with increasing number of laser pulses, while the magnitude of the second peak attributed to the contribution of Ag-Ag bonds, increases.

To confirm these qualitative conclusions, experimental Ag *K*-edge EXAFS in Samples 2—5000 were processed by the technique of [23], which enables to reduce the effect of correlations among fitting parameters on the determined values of structural

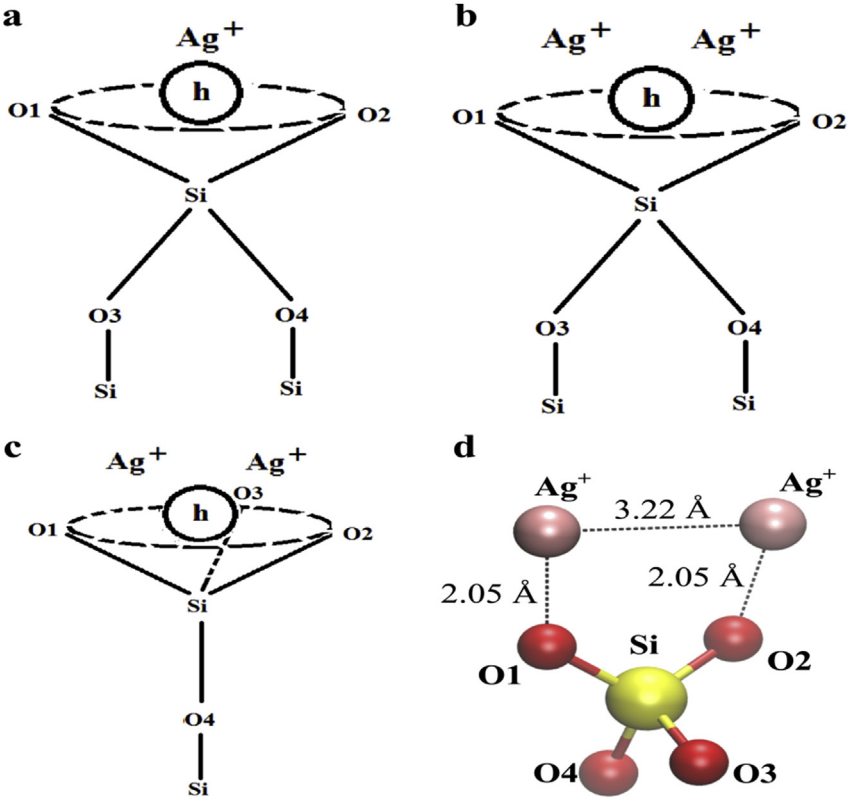

Fig. 7. Models of HTC structure in Ag^+ doped silicate glass: (a)–(c) – schematic illustration according to [28], where O1, O2 in (a)–(c) and O3 in (c) are the non-bridging oxygen atoms; (d) – atomic structure obtained by DFT calculations, which corresponds to scheme (b).

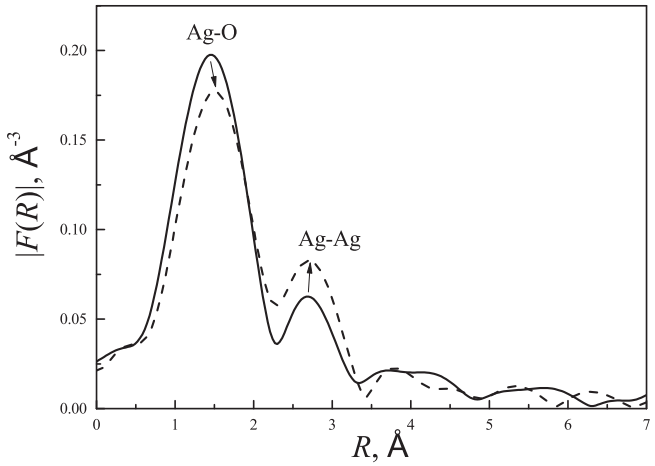

Fig. 8. FT magnitudes $|F(R)|$ of experimental Ag *K*-edge EXAFS in Sample 20 (solid curve) and in Sample 5000 (dashed curve).

parameters by using interdependencies between all correlating parameters of a fitting model, obtained at different weights k^n ($n = 0, 1, 2$) for oscillatory part $\chi^{exp}(k)$ of EXAFS and at different Δk intervals for Fourier transformation. The fit of $F(R)$ of EXAFS spectrum can be performed using the following expression for $\chi(k)$:

$$\chi(k) = A_{\mathrm{Ag-Ag}} \cdot \chi_{\mathrm{Ag-Ag}} + A_{\mathrm{Ag-O}} \cdot \chi_{\mathrm{Ag-O}} + \tilde{\chi}_{\mathrm{Ag}} \quad (5)$$

where $\chi_{\mathrm{Ag\text{-}Ag}}$ – is the contribution of one atomic pair Ag-Ag without the reduction factor S_0^2(Ag-Ag) [37] and $\chi_{\mathrm{Ag\text{-}O}}$ – is the contribution of one atomic pair Ag-O without S_0^2(Ag-O). These reduction factors are included into the amplitudes $A_{\mathrm{Ag\text{-}Ag}} = C_{\mathrm{Ag\text{-}Ag}} {}^{*} N_{\mathrm{Ag\text{-}Ag}} {}^{*} S_0^2$(Ag-Ag) and $A_{\mathrm{Ag\text{-}O}} = C_{\mathrm{Ag\text{-}O}} {}^{*} N_{\mathrm{Ag\text{-}O}} {}^{*} S_0^2$(Ag-O), where $C_{\mathrm{Ag\text{-}Ag}}$ and $C_{\mathrm{Ag\text{-}O}}$ are the fractions of Ag atoms in the sample bonded respectively with Ag and O atoms. $N_{\mathrm{Ag\text{-}Ag}}$ and $N_{\mathrm{Ag\text{-}O}}$ are respectively the number of Ag and O atoms neighboring to the absorbing Ag atom. In (5), $\tilde{\chi}_{\mathrm{Ag}}$ is the contribution of photoelectron scattering on the second and more distant coordination shells of the absorbing Ag atom. Determining structural parameters for the nearest neighbors of absorbing Ag atoms in the studied glass samples using the FT of EXAFS, allows to neglect the contribution of the last term $\tilde{\chi}_{Ag}(k)$ in (5). This can be done because in the small noble and transition metals NPs ($D \leq 3$ nm) the percentage of the near surface atoms is larger than those which can be attributed to the core [30]. Because of the increasing number of defects in the near surface region of NPs, the nearest surrounding of these atoms is characterized by the strong dispersion of the radii of the second and more distant shells and hence, in the reduction of their contributions in relation to the nearest neighbor ones, especially within the *R*-range of the nearest neighbors of the absorbing atom [38,39]. The fit of $F(R)$ of Ag *K*-edge EXAFS in the studied samples was performed by such a "nearest neighbors" approximation in (5). Comparison of the experimental Ag *K*-edge XANES in Ag-foil and in the studied glass samples revealed no significant (≥1 eV) energy shifts in the positions of their *K*-edges and therefore the functions $\chi(k)$ of the foil and of Samples 2–5000 were obtained in identical *k*-scales with the zero at the inflection point $E_0 = 25513$ eV. The *R*-space fit, performed in the range 0.5–3.5 Å gave average values of the following structural and non-structural parameters: partial amplitudes $A_{\mathrm{Ag\text{-}Ag}}$, $A_{\mathrm{Ag\text{-}O}}$ and corresponding Debye-Waller (DW) parameters $\sigma^2_{\mathrm{Ag-Ag}}$, $\sigma^2_{\mathrm{Ag-O}}$, interatomic distances $R_{\mathrm{Ag\text{-}Ag}}$, $R_{\mathrm{Ag\text{-}O}}$, and energy-shift parameters e_0(Ag-Ag), $e_0(Ag{-}O)$ [37]. For all samples, the obtained values $\sigma^2_{\mathrm{Ag-Ag}} \approx 0.008$ Å^2 and $\sigma^2_{\mathrm{Ag-O}} \approx 0.006$ Å^2 remained stable, while the values of parameters e_0 changed within the ranges: e_0(Ag-Ag) = 4.5 ± 1.5 eV and e_0(Ag-O) = −1.8 ± 0.3 eV.

Fig. 9 shows the dependences of amplitudes $A_{\mathrm{Ag\text{-}Ag}}$ and $A_{\mathrm{Ag\text{-}O}}$ upon the number *N* of laser pulses. As can be seen, both curves are approximately linear functions of lg(*N*). However, $A_{\mathrm{Ag\text{-}Ag}}$ increases with *N*, while $A_{\mathrm{Ag\text{-}O}}$ decreases. The corresponding conclusions can be made for the dependences of the fractions of Ag atoms in the sample bonded with Ag atoms ($C_{\mathrm{Ag\text{-}Ag}}$) and with O atoms ($C_{\mathrm{Ag\text{-}O}}$). This can be done, since i) according to XRD data, single particles sizes are not changed significantly with increasing *N* and, therefore, it is reasonable to use $N_{\mathrm{Ag\text{-}Ag}} \approx const$; ii) in Ag *K*-edge EXAFS analysis of silver nanoparticles one can neglect the interaction of surface Ag atoms of particles with oxygen atoms of the glass matrix [23] and therefore, it is also reasonable to use $N_{\mathrm{Ag\text{-}O}} \approx const$ irrespective of the number of laser pulses *N*.

In Fig. 10 the dependences of interatomic distances $R_{\mathrm{Ag\text{-}Ag}}$ and $R_{\mathrm{Ag\text{-}O}}$ upon the number *N* of laser pulses are presented. These two curves are very informative since each of them reflects the decrease in the amount of initially dominating silver ions owing to their reduction to neutral atoms Ag^0 according to the reaction $Ag^+ + e \rightarrow Ag^0$ by capturing electron from non-bridging oxygen bonds in a SiO_4 tetrahedron, which can be formed also under UV radiation [15,17]. Thus, considering the dependence of $R_{\mathrm{Ag\text{-}O}}$ upon *N*, one must take into account that the value $R_{\mathrm{Ag\text{-}O}} = 2.1$ Å in Sample 10 ($N = 10$ pulses) is typical for the bonds Ag^+–O and Ag^{3+}–O in different silver oxides, varying from 2.05 to 2.1 Å [40,41], whereas the value $R_{\mathrm{Ag\text{-}O}} = 2.15$ Å in Sample 5000 ($N = 5000$ pulses) is closer to interatomic Ag^0–O distances (2.16 Å) and longer ones, between Ag atoms of the particles surface and the nearest O atoms [42].

Interpretation of the dependence of $R_{\mathrm{Ag\text{-}Ag}}$ upon the number *N* of laser pulses (solid curve in Fig. 10) seems to be more complicated because in the glass samples after $Ag^+ \leftrightarrow Na^+$ ion exchange and irradiation with a small number of laser pulses one can expect the predominance of Ag-Ag interactions. These can be attributed to the most plausible color centers in glass: dimers Ag^+–Ag^+, Ag^+–Ag^0 [32] and HTC [28], simultaneously with clusters of neutral atoms Ag^0_n and small silver nanoparticles. The available data [43] and the results of DFT modeling of HTC of Sec. 3.3, enable us to conclude that the centers containing two silver ions are characterized by values of $R_{\mathrm{Ag\text{-}Ag}}$ distributed from ~2.9 to 3.3 Å. However, in small clusters Ag^0_n ($n = 2$–15 atoms) the value of $R_{\mathrm{Ag\text{-}Ag}}$ increases from 2.69 Å for $n = 2$ [41] to 2.75 Å for $n = 15$ atoms [44], reaches ~ 2.87 Å in small silver nanoparticles of sizes $D < 5$ nm [23] and is then approaching its crystalline limit (2.89 Å) in nanoparticles of sizes $D > 10$ nm [30]. According to these data, the interval of Ag-Ag distances between the nearest neighbors can be approximately divided into two parts with a boundary at $R_{\mathrm{Ag\text{-}Ag}}$ ~2.85–2.9 Å, where the low-$R_{\mathrm{Ag\text{-}Ag}}$ region can be attributed to Ag^0–Ag^0 bonds,

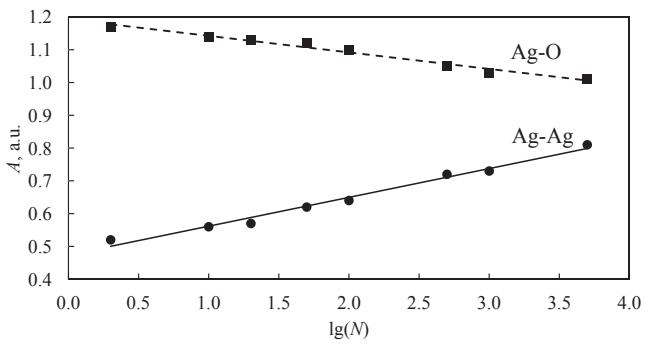

Fig. 9. Dependences of amplitudes (*A*) of Ag-Ag (solid curve) and Ag-O (dashed curve) interactions upon the number *N* of laser pulses.

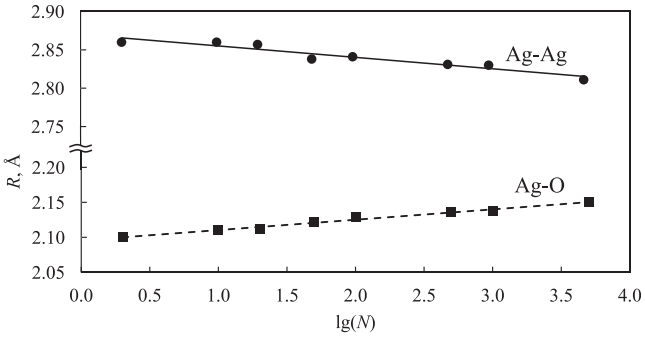

Fig. 10. Dependences of interatomic distances (R) of Ag-Ag (solid curve) and Ag-O (dashed curve) bonds upon the number N of laser pulses.

while the higher $R_{Ag\text{-}Ag}$ region corresponds to Ag^+–Ag^+ interactions.

By using such a partition of Ag-Ag distances and accounting for the simultaneous presence of both ionic and neutral silver atoms constructions in the samples, one can conclude that the obtained largest value of $R_{Ag\text{-}Ag} = 2.86$ Å for samples 10 and 20 (low numbers of laser pulses) is the result of the averaging over the predominant number of Ag^+–Ag^+ interactions and the small enough number of Ag^0–Ag^0 bonds, belonging to the silver clusters and small nanoparticles. The decrease of $R_{Ag\text{-}Ag}$ with increasing number N of laser pulses can then be explained as a decrease in the number of silver ions due to their reduction, simultaneously with an increase of contribution of neutral silver atoms constructions (small clusters and nanoparticles) to the formation of the average EXAFS signal.

4. Conclusions

The study of silver nanoparticles formation in soda-lime glass, doped by silver through $Ag^+ \leftrightarrow Na^+$ ion exchange and irradiated by UV laser with varied number of pulses, was performed by the methods, which provided the obtaining of complementary information: i) on the formation of silver NPs and their following aggregation (optical spectroscopy measurements, considering SPR); ii) on NPs sizes and size distribution (HRTEM and XRD); iii) on the parameters of atomic structure of silver NPs and Ag-O bonds (XRD and EXAFS spectroscopy). Analysis of HRTEM micrographs, changes in XRD patterns, in optical absorption spectra and EXAFS in glass samples, laser irradiated with increasing number of pulses from 10 to 5000, lead to the following conclusions:

– in soda-lime silicate glasses after $Ag^+ \leftrightarrow Na^+$ ion exchange at 330 °C during 20 min, approximately 50% of the sodium ions are replaced by silver ions. Besides the silver ions, there exist silver centers containing Ag^0 species and very small (<3 nm) silver nanoparticles;
– irradiation of such glass-samples with a UV laser leads to the formation of separated crystalline silver nanoparticles with the size ≤ 3 nm inside the glass matrix as well as larger agglomerations (≥5 nm) of small particles, detected by HRTEM. The number of such aggregates increases with the increasing number of laser pulses, simultaneously with a reduction in the number of silver ions, which is reflected in Ag-Ag and Ag-O structural parameters obtained from EXAFS.
– a broad line at ~450 nm in optical absorption spectra of glass samples, prepared with a small number of laser pulses (≤100) can be attributed to the SPR and to absorption by HTC and NBOHC species formed under UV irradiation. The increasing number of larger Ag agglomerations or the increasing size of such aggregates with increasing number of laser pulses up to 5000 leads to the formation of a distinct SPR line at ~435 nm;
– DFT modeling of a HTC with two nearest silver ions in silicate glass yielded an estimate of structural parameters of the HTC, including the interatomic Ag-Ag and Ag-O distances.

The combination of the used methods seems to be promising in the study of laser irradiated Ag^0 atoms and Ag particle formation to achieve an enhanced control of the SPR parameters in metal-doped glass modifications for photonic applications.

Acknowledgements

The work was supported by DFG-RFBR project (DFG No DU 214/14-1, RFBR No 14-02-91334).

Authors are thankful for XAFS measurements to Structural Materials Science beamline of the Kurchatov Synchrotron Radiation Source (NRC "Kurchatov Institute", Moscow, Russia) and to Dr. A. Guda and K. Lomachenko for the help in XRD measurements at BM01B beamline of ESRF (Grenoble, France).

References

[1] M.I. Stockman, Nanoplasmonics: past, present, and glimpse into future, Opt. Express 19 (2011) 22029–22106, http://dx.doi.org/10.1364/OE.19.022029.
[2] V. Torres, M. Popa, D. Crespo, J.M. Calderón Moreno, Silver nanoprism coatings on optical glass substrates, Microelectron. Eng. 84 (2007) 1665–1668, http://dx.doi.org/10.1016/j.mee.2007.01.262.
[3] R.M. Mohamed, I.A. Mkhalid, Characterization and catalytic properties of nano-sized Ag metal catalyst on TiO2–SiO2 synthesized by photo-assisted deposition and impregnation methods, J. Alloys Compd. 501 (2010) 301–306, http://dx.doi.org/10.1016/j.jallcom.2010.04.092.
[4] O. Véron, J.-P. Blondeau, M. Grabiec, A. Wolak, K. Dzierżęga, N. Ollier, et al., On-line optical and morphological studies of silver nanoparticles growth formed by nanosecond laser irradiation of silver-exchanged silicate glass, Plasmonics 8 (2012) 93–103, http://dx.doi.org/10.1007/s11468-012-9427-4.
[5] V. Amendola, O.M. Bakr, F. Stellacci, A study of the surface plasmon resonance of silver nanoparticles by the discrete dipole approximation method: effect of shape, size, structure, and assembly, Plasmonics 5 (2010) 85–97, http://dx.doi.org/10.1007/s11468-009-9120-4.
[6] M. Dubiel, J. Haug, H. Kruth, H. Hofmeister, K.-D. Schicke, Ag/Na ion exchange in soda-lime glasses and the formation of small Ag nanoparticles, Mater. Sci. Eng. B 149 (2008) 146–151, http://dx.doi.org/10.1016/j.mseb.2007.11.035.
[7] M. Dubiel, S. Brunsch, U. Kolb, D. Gutwerk, H. Bertagnolli, Experimental studies investigating the structure of soda-lime glasses after silver-sodium ion exchange, J. Non Cryst. Solids 220 (1997) 30–44, http://dx.doi.org/10.1016/S0022-3093(97)00230-5.
[8] M. Dubiel, R. Schmitz, U. Kolb, D. Gutwerk, H. Bertagnolli, X-ray diffraction and absorption studies of ion exchanged glasses, Phys. B Condens. Matter 208–209 (1995) 349–350, http://dx.doi.org/10.1016/0921-4526(94)00694-Q.
[9] S. Mohapatra, Tunable surface plasmon resonance of silver nanoclusters in ion exchanged soda lime glass, J. Alloys Compd. 598 (2014) 11–15, http://dx.doi.org/10.1016/j.jallcom.2014.02.021.
[10] M. Dubiel, M. Heinz, M. Stiebing, J. Meinertz, J. Ihlemann, T. Rainer, Generation and characterization of plasmonic nanostructures in glass surfaces by means of excimer and solid state laser irradiation, in: A.D. Boardman (Ed.), SPIE Nanosci. + Eng, International Society for Optics and Photonics, 2014, p. 91631M, http://dx.doi.org/10.1117/12.2061034.
[11] M. Grabiec, A. Wolak, O. Véron, J.-P. Blondeau, N. Pellerin, M. Allix, et al., Laser-driven precipitation and modification of silver nanoparticles in soda lime glass matrix monitored by on-line extinction measurements, Plasmonics 7 (2011) 279–286, http://dx.doi.org/10.1007/s11468-011-9304-6.
[12] E. Trave, F. Gonella, P. Calvelli, E. Cattaruzza, P. Canton, D. Cristofori, et al., Laser beam irradiation of silver doped silicate glasses, Nucl. Instrum. Methods Phys. Res. Sect. B Beam Interact. Mater. Atoms 268 (2010) 3177–3182, http://dx.doi.org/10.1016/j.nimb.2010.05.082.
[13] F. Goutaland, M. Sow, N. Ollier, F. Vocanson, Growth of highly concentrated silver nanoparticles and nanoholes in silver-exchanged glass by ultraviolet continuous wave laser exposure, Opt. Mater. Express 2 (2012) 350, http://dx.doi.org/10.1364/OME.2.000350.
[14] A.L. Stepanov, D.E. Hole, P.D. Townsend, Modification of size distribution of ion implanted silver nanoparticles in sodium silicate glass using laser and thermal annealing, Nucl. Instrum. Methods Phys. Res. Sect. B Beam Interact. Mater. Atoms 149 (1999) 89–98, http://dx.doi.org/10.1016/S0168-583X(98)90733-9.
[15] H. Hosono, K. Kajihara, T. Suzuki, Y. Ikuta, L. Skuja, M. Hirano, Vacuum ultraviolet absorption band of non-bridging oxygen hole centers in SiO2 glass, Solid State Commun. 122 (2002) 117–120.

[16] E. Trave, E. Cattaruzza, F. Gonella, P. Calvelli, A. Quaranta, A. Rahman, et al., Ag clustering investigation in laser irradiated ion-exchanged glasses by optical and vibrational spectroscopy, Appl. Surf. Sci. 258 (2012) 9399–9403, http://dx.doi.org/10.1016/j.apsusc.2011.09.084.
[17] J. Zhang, W. Dong, J. Sheng, J. Zheng, J. Li, L. Qiao, et al., Silver nanoclusters formation in ion-exchanged glasses by thermal annealing, UV-laser and X-ray irradiation, J. Cryst. Growth 310 (2008) 234–239, http://dx.doi.org/10.1016/j.jcrysgro.2007.10.007.
[18] Tanvi, A. Mahajan, R.K. Bedi, S. Kumar, V. Saxena, D.K. Aswal, Effect of the crystallinity of silver nanoparticles on surface plasmon resonance induced enhancement of effective absorption cross-section of dyes, J. Appl. Phys. 117 (2015) 083111, http://dx.doi.org/10.1063/1.4913713.
[19] Y. Battie, N. Destouches, L. Bois, F. Chassagneux, A. Tishchenko, S. Parola, et al., Growth mechanisms and kinetics of photoinduced silver nanoparticles in mesostructured hybrid silica films under UV and visible illumination, J. Phys. Chem. C 114 (2010) 8679–8687, http://dx.doi.org/10.1021/jp9046903.
[20] U. Kreibig, M. Vollmer, Optical Properties of Metal Clusters, Springer Berlin Heidelberg, Berlin, Heidelberg, 1995, http://dx.doi.org/10.1007/978-3-662-09109-8.
[21] K.F.E. Williams, C.E. Johnson, O. Nikolov, M.F. Thomas, J.A. Johnson, J. Greengrass, Characterization of tin at the surface of float glass, J. Non Cryst. Solids 242 (1998) 183–188, http://dx.doi.org/10.1016/S0022-3093(98)00799-6.
[22] G.H. Frischat, Tin ions in float glass cause anomalies, Comptes Rendus Chim. 5 (2002) 759–763, http://dx.doi.org/10.1016/S1631-0748(02)01436-4.
[23] V.V. Srabionyan, A.L. Bugaev, V.V. Pryadchenko, A.V. Makhiboroda, E.B. Rusakova, L.A. Avakyan, R. Schneider, M. Dubiel, L.A. Bugaev, EXAFS study of changes in atomic structure of silver nanoparticles in soda-lime glass caused by annealing, J. Non Cryst. Solids 382 (2013) 24–31, http://dx.doi.org/10.1016/j.jnoncrysol.2013.09.025.
[24] H. Bach, F.G.K. Baucke, Ultraviolet absorption spectra of the Ag+ ion in glass, Phys. Chem. Glasses 27 (1986) 215–217.
[25] E. Borsella, G. Battaglin, M.A. Garcìa, F. Gonella, P. Mazzoldi, R. Polloni, et al., Structural incorporation of silver in soda-lime glass by the ion-exchange process: a photoluminescence spectroscopy study, Appl. Phys. A. 71, n.d., 125–132. doi: 10.1007/PL00021106.
[26] U. Kreibig, Small silver particles in photosensitive glass: their nucleation and growth, Appl. Phys. 10 (1976) 255–264, http://dx.doi.org/10.1007/BF00897225.
[27] M. Quinten, U. Kreibig, D. Schonauer, L. Genzel, Optical absorption spectra of pairs of small metal particles, Surf. Sci. Lett. 156 (1985), http://dx.doi.org/10.1016/0167-2584(85)90462-1. A333-A333.
[28] J.W.H. Schreurs, Study of some trapped hole centers in x-irradiated alkali silicate glasses, J. Chem. Phys. 47 (1967) 818–830, http://dx.doi.org/10.1063/1.1711956.
[29] Y. Shimotsuma, K. Hirao, P.G. Kazansky, J. Qiu, Three-dimensional micro- and nano-fabrication in transparent materials by femtosecond laser, Jpn. J. Appl. Phys. 44 (2005) 4735–4748, http://dx.doi.org/10.1143/JJAP.44.4735.
[30] V.V. Srabionyan, A.L. Bugaev, V.V. Pryadchenko, L.A. Avakyan, J.A. Van Bokhoven, L.A. Bugaev, EXAFS study of size dependence of atomic structure in palladium nanoparticles, J. Phys. Chem. Solids 75 (2014) 470–476.
[31] L. Yu, Y. Shi, Z. Zhao, H. Yin, Y. Wei, J. Liu, et al., Ultrasmall silver nanoparticles supported on silica and their catalytic performances for carbon monoxide oxidation, Catal. Commun. 12 (2011) 616–620, http://dx.doi.org/10.1016/j.catcom.2010.12.012.
[32] W. Zheng, T. Kurobori, Assignments and optical properties of X-ray-induced colour centres in blue and orange radiophotoluminescent silver-activated glasses, J. Lumin. 131 (2011) 36–40, http://dx.doi.org/10.1016/j.jlumin.2010.08.024.
[33] P.A. Obraztsov, A.V. Nashchekin, N.V. Nikonorov, A.I. Sidorov, A.V. Panfilova, P.N. Brunkov, Formation of silver nanoparticles on the silicate glass surface after ion exchange, Phys. Solid State 55 (2013) 1272–1278, http://dx.doi.org/10.1134/S1063783413060267.
[34] J.P. Perdew, K. Burke, M. Ernzerhof, Generalized gradient approximation made simple, Phys. Rev. Lett. 77 (1996) 3865–3868, http://dx.doi.org/10.1103/PhysRevLett.77.3865.
[35] M. Valiev, E.J. Bylaska, N. Govind, K. Kowalski, T.P. Straatsma, H.J.J. Van Dam, et al., NWChem: a comprehensive and scalable open-source solution for large scale molecular simulations, Comput. Phys. Commun. 181 (2010) 1477–1489, http://dx.doi.org/10.1016/j.cpc.2010.04.018.
[36] J. Sheng, J. Zheng, J. Zhang, C. Zhou, L. Jiang, UV-laser-induced nanoclusters in silver ion-exchanged soda-lime silicate glass, Phys. B Condens. Matter 387 (2007) 32–35, http://dx.doi.org/10.1016/j.physb.2006.03.024.
[37] D.C. Koningsberger, B.L. Mojet, G.E. van Dorssen, D.E. Ramaker, XAFS spectroscopy; fundamental principles and data analysis, Top. Catal. 10 (2000) 143–155, http://dx.doi.org/10.1023/A:1019105310221.
[38] L.A. LaJohn, P.A. Christiansen, R.B. Ross, T. Atashroo, W.C. Ermler, Ab initio relativistic effective potentials with spin–orbit operators. III. Rb through Xe, J. Chem. Phys. 87 (1987) 2812, http://dx.doi.org/10.1063/1.453069.
[39] V.V. Pryadchenko, V.V. Srabionyan, E.B. Mikheykina, L.A. Avakyan, V.Y. Murzin, Y.V. Zubavichus, I. Zizak, V.E. Guterman, L.A. Bugaev, Atomic structure of bimetallic nanoparticles in PtAg/C catalysts: determination of components distribution in the range from disordered alloys to “Core–Shell” structures, J. Phys. Chem. C 119 (2015) 3217–3227, http://dx.doi.org/10.1021/jp512248y.
[40] J.A. McMillan, Magnetic properties and crystalline structure of AgO, J. Inorg. Nucl. Chem. 13 (1960) 28–31, http://dx.doi.org/10.1016/0022-1902(60)80231-X.
[41] J.P. Allen, D.O. Scanlon, G.W. Watson, Electronic structures of silver oxides, Phys. Rev. B 84 (2011) 115141, http://dx.doi.org/10.1103/PhysRevB.84.115141.
[42] Y. Wang, L. Jia, W. Wang, K. Fan, O/Ag(100) surface: a density functional study with slab model, J. Phys. Chem. B 106 (2002) 3662–3667, http://dx.doi.org/10.1021/jp012552p.
[43] Y.I. Tarasov, Z.G. Bazhanova, D.M. Kovtun, A.I. Boltalin, B.K. Novosadov, I.V. Kochikov, Quantum-chemical study of the silver trifluoroacetate dimer, J. Struct. Chem. 49 (2008) 207–215, http://dx.doi.org/10.1007/s10947-008-0116-2.
[44] P. Weis, T. Bierweiler, S. Gilb, M.M. Kappes, Structures of small silver cluster cations (Agn+, n <12): ion mobility measurements versus density functional and MP2 calculations, Chem. Phys. Lett. 355 (2002) 355–364, http://dx.doi.org/10.1016/S0009-2614(02)00277-4.